CrossMark

RESEARCH PAPER

Friction factor in nanochannel flows

Antonios Liakopoulos[1] · Filippos Sofos[1] · Theodoros E. Karakasidis[1]

Abstract Non-equilibrium molecular dynamics simulations are employed in order to access the detailed atomic behavior of fluids moving in nanochannels and to quantify the associated energy dissipation. Nanochannels of various degrees of wall hydrophobicity/hydrophilicity and roughness are studied. Dimensional arguments that include the role of the atomistic model parameters allow us to derive a functional expression for the Darcy–Weisbach friction factor, f, so that macroscopic flow estimates of f can be compared to those for nanochannel flows. The NEMD simulations allow us to take into account parameters such as wall/fluid interaction which are neglected in the macroscopic theories and embed proposed modifications in classical relations. The methodology forms the basis for generating Moody's-like diagrams for nanoscale conduit flows where the range of the relative roughness parameter is significantly larger than in macroflows.

List of symbols

A	Cross-sectional area in a channel
D	Diffusion coefficient
D_h	Hydraulic diameter
f	Darcy–Weisbach friction factor
f_{ext}	Magnitude of external driving force
h	Channel width
h_{av}	Theoretical channel width
h_l	Wall roughness length
h_d	Wall roughness height
H_{loss}	Energy loss per unit mass
$\mathbf{J}_p$	Microscopic stress tensor
K	Spring constant
k_B	Boltzman constant
L	Length of a channel segment
M	Total mass
m	Particle mass
N	Number of particles
$\mathbf{r}_{eq}$	Position of a wall atom on fcc lattice site
$\mathbf{r}_i$	Position vector of atom i
$\mathbf{r}_{ij}$	Distance vector between ith and jth atom
Re	Reynolds number
T	Temperature
$u(r_{ij})$	LJ potential of atom i with atom j
V	Volume
v	Average fluid velocity at a channel cross-section

Greek symbols

$\dot{\gamma}$	Strain rate
Δp	Pressure drop
ε_f	Fluid energy parameter in the LJ potential
ε_w	Wall energy parameter in the LJ potential
θ	Contact angle
μ	Coefficient of shear viscosity
ν	Coefficient of kinematic viscosity
ρ_f	Fluid density
ρ_w	Wall density
σ_f	Fluid length parameter in the LJ potential
σ_w	Wall length parameter in the LJ potential

✉ Theodoros E. Karakasidis
thkarak@uth.gr

[1] Laboratory of Hydromechanics and Environmental Engineering, Department of Civil Engineering, School of Engineering, University of Thessaly, Pedion Areos, 38834 Vólos, Greece

1 Introduction

Attention has grown in the last decades on the nanoscale regime of fluid mechanics as the scientific community re-investigates the classical theory and tries to bridge models at different scales, in order to understand the complex mechanisms involved in solid/fluid interactions. Theoretical and experimental studies in fields such as carbon dioxide separation, drug delivery, friction and lubrication, membrane science, water desalination and purification, have been embedded in innovative technological applications (Bernardo et al. 2009; Gargiuli et al. 2006; Grannick 1991; Kleinstreuer et al. 2008; Noy et al. 2007; Walther et al. 2013; Asproulis et al. 2012). However, there are still numerous ambiguities to be resolved as far as the limits of applicability of classical theory on micro- and nanoflows are concerned.

For pipe flows, as dimensions decrease dramatically, the impact of surface roughness is significant. Moody's diagram (Moody 1944) is a point of reference, as a convenient method of determining the pressure drop in macroscopic pipe flows and has been extended to conduits of non-circular cross-section. In the analysis by Kandlikar et al. (2005), suggestions are made to the extension of the Moody diagram by incorporating three additional geometrical parameters of roughness. Herwig et al. (2008) tried to provide a theoretical background to the well-established experimental measurements (Nikuradse 1933) that constitute most of the information incorporated in the diagram. In the work of Valdés et al. (2007, 2008) a numerical model is proposed, where wall roughness is substituted by appropriate factors embedded in a respective smooth (flat-wall) channel.

The effect of surface roughness on micro- and nanoflows has been studied extensively over the last decade, mainly because of the finding, in both theoretical studies and experimental proves, that the classical hypothesis of the no-slip condition breaks down when downsizing to the micro/nanoscale. Davies et al. (2006) showed that, under specific rough-wall characteristics, significant reductions in the frictional pressure drop and greater effective fluid slip at the walls can be achieved relative to the classical smooth channel Stokes flow. Priezjev (2007) noticed that slip length reduces by periodic and random surface roughness, compared to atomically smooth rigid walls, while in Sofos et al. (2012) it is observed that roughness geometrical characteristics could affect slip length values, through fluid atom trapping inside the grooves. Wall roughness is also induced by wall particle oscillating frequencies and, along with wall mass; it is found to connect with slip length (Asproulis and Drikakis 2011). Experimental work reveals how large surface roughness must be to produce the no-slip boundary condition (Zhu and Granick 2002), while in Tretheway and Meinhart (2002) it is noted that fluid slip exists at small scales under the limit of 1 mm.

The effect of surface characteristics on flows is not only limited to roughness. Terms like super- or ultra-hydrophobic surfaces have been incorporated in order to describe hydrophobic surfaces (and rough at the same time) where the contact angle, θ, is greater than 150° (Cao et al. 2011). It is also noted that the slip length can be considered as a quantity used to quantify hydrophobicity at the micro- or nanoscale (Voronov et al. 2006; Koplik and Banavar 2006); however, for super-hydrophobic surfaces, hydrophobicity and roughness have a coupled effect (Sbragaglia et al. 2006). In Maynes et al. (2007), a dramatic decrease in the overall flow resistance is observed due to reduction in the surface contact area between the flowing liquid and the solid (hydrophobic, patterned) wall. Ybert et al. (2007) presented a method of calculating frictional properties of super-hydrophobic surfaces as a function of the generic geometrical parameters of the surface and showed that very large slip lengths can be obtained for an ultra-hydrophobic surface ($\theta \approx 180°$).

However, the contact angle θ is not sufficient to infer the amount of slip. For example, it was shown that there are cases where strongly super-hydrophobic fractal-patterned surfaces may be not efficient in terms of drag reduction (Cottin-Bizonne et al. 2012). The effect of the size and geometrical characteristics of wall protrusions, wall wettability and wall stiffness on nanochannel flows is intensified by the channel width, h, which is the main parameter that controls how close or far from the continuum regime we are.

In the present work, we calculate the Darcy–Weisbach friction factor, f, based on data compiled from molecular dynamics simulations. We focus mainly: (a) on how wall hydrophobicity/hydrophilicity affects f and (b) on quantifying the effect of wall roughness on f. Dimensional analysis is applied in order to derive correlations for the friction factor. The results show that construction of Moody-like diagrams is possible in the case of nanochannels, provided that some appropriate modifications related to the scale characteristics are taken into account. Furthermore, the clustering of the computed friction factor values allows us to delineate the rough-wall regime from the grooved-wall regime, at least for the particular idealized form of orthogonal wall protrusions studied in the present work. Our investigation could also serve as an intermediate step toward a hybrid (atomistic and continuum) simulation design (Asproulis and Drikakis 2013; Kalweit and Drikakis 2010).

2 Theoretical relations and modeling

2.1 Molecular dynamics simulations

The Lennard-Jones (LJ) 12-6 type potential, $u^{LJ}(r_{ij}) = 4\varepsilon\left[(\sigma/r_{ij})^{12} - (\sigma/r_{ij})^6\right]$, is widely used to describe interatomic interaction within the non-equilibrium molecular

dynamics (NEMD) method. Monoatomic LJ particles (argon) are incorporated for walls and fluid, with $\sigma_f = \sigma_w = \sigma = 0.3405$ nm, $\varepsilon_f/k_B = \varepsilon_w/k_B = \varepsilon/k_B = 119.8$ K, fluid density $\rho_f = 1078$ kg/m^3 and wall density $\rho_w = 1477$ kg/m^3. The simulation cell resembles a flat-wall nanochannel (Fig. 1), which is equivalent to macroscopic Poiseuille flow. The system is periodic along the x- and y-directions, while the distance, h, between the two walls is examined for $h = 3.15$ and 6.3 nm, i.e., 9.3 and 18.6σ, respectively. The respective hydraulic diameter is $D_h = 2h$.

We also investigate monoatomic LJ liquid flow in rough-wall simulation cells (Fig. 1), with periodic grooves of various length and height, h_l and h_d, respectively. The simulation cases studied here involve roughness length $h_l = 1.8$ nm and various roughness heights, $0.6 \leq h_d \leq 1.96$ nm, which correspond to $h_d = 5$–20 %h. We choose the theoretical channel width as $h_{av} = h - h_d/2$, so the hydraulic diameter is $D_h = 2h_{av} = 2h - h_d$. A qualitative wall wettability parameter representing hydrophobic or hydrophilic behavior is $\varepsilon_{wall}/\varepsilon_{fluid}$ (from now on, $\varepsilon_w/\varepsilon_f$). We investigate wall wettability effect over the range $0.1 < \varepsilon_w/\varepsilon_f < 1.0$.

The wall/fluid interaction is a means of characterizing the degree of wall wettability. In Cao et al. (2009), wettability is characterized by the contact angle θ (taken from Young's Law, $\cos\theta = -1 + 2\frac{\rho_S c_{LS}}{\rho_L c_{LL}}$, where ρ is density and subscripts S and L indicate solid wall and fluid, respectively) which, in turn, depends on a constant c embedded in the original LJ equation, $u^{LJ}(r_{ij}) = 4\varepsilon((\sigma/r_{ij})^{12} - c(\sigma/r_{ij})^6)$. In Voronov et al. (2006), by varying the relative energy parameter $\varepsilon_r = \varepsilon_{wf}/\varepsilon_f$, the authors change the wall affinity from hydrophilic (large e_r) to hydrophobic (small e_r), and this is analogous to the contact angle change. Our method is similar to Voronov et al. (2006), where if Lorentz–Berthelot rule applies, then $\varepsilon_r = \varepsilon_{wf}/\varepsilon_f = \sqrt{\varepsilon_w \cdot \varepsilon_f}/\varepsilon_f = \sqrt{\frac{\varepsilon_w}{\varepsilon_f}}$. Furthermore, in Sofos et al. (2012), potential energy contours near the walls show that a large $\varepsilon_w/\varepsilon_f$ ratio leads in increased fluid atom presence near the walls (hydrophilic wall), while a small $\varepsilon_w/\varepsilon_f$ ratio leads in decreased fluid atom presence near the walls (hydrophobic wall).

Wall atoms are bound on fcc (101) sites and remain fixed to their original positions due to the effect of an elastic spring force $\mathbf{F} = -K(\mathbf{r}(t) - \mathbf{r}_{eq})$, where $\mathbf{r}(t)$ is the vector position of a wall atom at time t, $\mathbf{r}_{eq}$ is its initial lattice position vector, and $K = 0.816$ N/m, the wall spring constant. An external driving force f_{ext} is applied along the x-direction to every fluid particle during the simulation, with magnitude ranging from 0.009 to 0.045 pN. A Nosé–Hoover thermostat scheme is applied independently to each thermal wall to keep fluid temperature constant to $T = 120$ K.

2.2 Theoretical relations

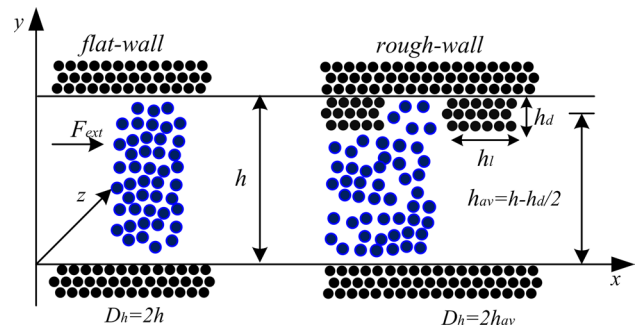The relation giving the Darcy–Weisbach friction factor is

Fig. 1 Model of flat-wall and rough-wall nanochannel

$$f = \frac{\left(\frac{\Delta p}{L}\right) D_h}{\frac{1}{2}\rho v^2} \qquad (1)$$

where ρ is the mass density, Δp denotes the pressure drop along a channel segment of length L, v is the average fluid velocity at a channel cross-section and D_h the hydraulic diameter. If V denotes the volume inside the channel and M the total mass between two successive channel cross-sections, then

$$f = \frac{\left(\frac{\Delta p}{L}\right) V D_h}{\frac{1}{2}M v^2} \qquad (2)$$

For fluid flows at the nanoscale, it is common to use periodic conditions for the channel in order to simulate the flow. The flow is driven not by a pressure difference Δp, but by an external force f_{ext} applied to each of the N fluid particles in the atomistic model. Consequently, $Nf_{ext} \leftrightarrow (\Delta p)A$, where A is the cross-sectional area. Equation (2) now becomes

$$f = \frac{Nf_{ext}\left(\frac{1}{A}\frac{V}{L}\right) D_h}{\frac{1}{2}M v^2} \qquad (3)$$

We note that $\frac{V}{AL} \approx 1$, so Eq. (3) becomes

$$f = \frac{f_{ext} D_h}{\frac{1}{2}\left(\frac{M}{N}\right)v^2} \qquad (4)$$

and by substituting the particle mass $m = M/N$ we obtain

$$f = \frac{f_{ext} D_h}{\frac{1}{2}m v^2} \qquad (5)$$

so that the friction factor can be calculated based on MD simulation parameters

The Reynolds number is defined here as

$$Re = \frac{v D_h}{\nu} \qquad (6)$$

or

$$Re = \frac{vD_{\mathrm{h}}}{\mu/\rho} \tag{7}$$

where ν is the coefficient of kinematic viscosity and μ the coefficient of shear viscosity.

Shear viscosity in nanochannels can be calculated by Green–Kubo (Sofos et al. 2009) or NEMD (Delhommelle et al. 2004; Sofos et al. 2010) relations. Green–Kubo methods are mainly used in systems close to or at equilibrium state, and they do not take into account the induced strain rates, while NEMD methods do. The Green–Kubo formula for shear viscosity μ_{GK} is

$$\mu_{\mathrm{GK}} = \frac{1}{\math\Psi k_{\mathrm{B}}T} \int_0^\infty dt \left\langle \mathbf{J}_{\mathrm{p}}^{xz}(t) \cdot \mathbf{J}_{\mathrm{p}}^{xz}(0) \right\rangle \tag{8}$$

where $\mathbf{J}_{\mathrm{p}}^{xy}$ is the off-diagonal component of the microscopic stress tensor

$$\mathbf{J}_{\mathrm{p}}^{xz} = \sum_{i=1}^N m_i v_i^x v_i^z - \sum_{i=1}^N \sum_{j>1}^N r_{ij}^x \frac{\partial u(r_{ij})}{\partial r_{ij}^z} \tag{9}$$

Shear viscosity μ_{NEMD} computed by NEMD methods is

$$\mu_{\mathrm{NEMD}} = \lim_{F_{\mathrm{ext}} \to 0} \left[-\frac{\langle J_{xz} \rangle}{\dot\gamma} \right] \tag{10}$$

where the strain rate $\dot\gamma$ is

$$\dot\gamma = \frac{\partial v_x}{\partial z} \tag{11}$$

However, there are cases where other methods have been employed. In Markesteijn et al. (2012) and Koplik et al. (1988), a method based on curve fitting that connects the MD with the continuum velocity profile is proposed, while continuum relations have been employed in Giannako-poulos et al. (2012), Ohara and Suzuki (2001), Ritos et al. (2014) and Thomas and McGaughey (2007). If the diffusion coefficient is known, equation

$$D = \frac{k_{\mathrm{B}}T}{\alpha \pi \mu \sigma} \tag{12}$$

relates D, μ and σ. Our results suggest that Eq. (12) can be used with constant $\alpha = 6$ for channels of width below $h = 5$ nm (lower bound, known as the Einstein equation), and $\alpha = 4$ (upper bound, known as the Sutherland equation) for about $h > 5$ nm. Equation (12) showed excellent agreement to our Green–Kubo calculations on shear viscosity (Giannakopoulos et al. 2012).

In previous works (Sofos et al. 2009, 2010), we employed diffusion coefficient calculations based on Einstein's relation

$$D = \lim_{t \to \infty} \frac{1}{6Nt} \left\langle \sum_{j=1}^N \left[\mathbf{r}_j(t) - \mathbf{r}_j(0) \right]^2 \right\rangle \tag{13}$$

The combination of Eqs. (12, 13) is used in this work for shear viscosity calculations in order to avoid complications coming from the induced strain rates due to various rough-wall channel geometries and hydrophobic/hydrophilic wall/fluid interactions.

2.3 Dimensional analysis

The energy loss per unit mass, H_{loss}, depends on the average cross-sectional velocity, v, the channel geometrical characteristics (h and h_{d}, or, equivalently D_{h}), the fluid properties (ρ, μ), as well as the atomistic model parameters (ε_{w}, ε_{f}, σ_{w}, σ_{f}, K^*, r_{c}). Simulation evidence supports the assumption that ε_{w}, ε_{f} are the most important atomistic parameters affecting H_{loss} in nanochannels, i.e., our starting point is that there exists a functional relation of the form.

$$H_{\mathrm{loss}} = g(v, D_{\mathrm{h}}, h_{\mathrm{d}}, \rho, \mu, \varepsilon_{\mathrm{w}}, \varepsilon_{\mathrm{f}}) \tag{14}$$

for the flows considered in this work.

A straightforward application of dimensional analysis of Eq. (14) yields five independent dimensionless groups: $\Pi_1 = H_{\mathrm{loss}} \frac{2D_{\mathrm{h}}}{Lv^2} = f$, $\Pi_2 = \frac{vD_{\mathrm{h}}}{\nu} = \frac{\rho vD_{\mathrm{h}}}{\mu} = Re$, $\Pi_3 = \frac{h_{\mathrm{d}}}{h}$, $\Pi_4 = \frac{\varepsilon_{\mathrm{w}}}{v^2 D_{\mathrm{h}}^3 \rho}$, $\Pi_5 = \frac{\varepsilon_{\mathrm{f}}}{v^2 D_{\mathrm{h}}^3 \rho}$, where f is the Darcy–Weisbach friction factor and Re is the Reynolds number. Consequently,

$$f = \hat{G}\left(Re, \frac{h_d}{D_h}, \Pi_4, \Pi_5\right) \tag{15}$$

or equivalently

$$f = \bar{G}\left(Re, \frac{h_{\mathrm{d}}}{D_{\mathrm{h}}}, \frac{\varepsilon_{\mathrm{w}}}{\varepsilon_{\mathrm{f}}}, \Pi_5\right) \tag{16}$$

where $\frac{\varepsilon_{\mathrm{w}}}{\varepsilon_{\mathrm{f}}} = \frac{\Pi_4}{\Pi_5} = \Pi_\varepsilon$.

We drop Π_5 in favor of $\Pi_\varepsilon = \frac{\varepsilon_{\mathrm{w}}}{\varepsilon_{\mathrm{f}}}$ as being more relevant and important dimensionless parameter in our analysis. Consequently, in the remainder of the paper we work with the non-dimensional functional relation

$$f = G\left(Re, \frac{h_{\mathrm{d}}}{D_{\mathrm{h}}}, \frac{\varepsilon_{\mathrm{w}}}{\varepsilon_{\mathrm{f}}}\right) \tag{17}$$

3 Calculated results

3.1 Shear viscosity

Figure 2 displays shear viscosity values over each flow parameter investigated. Shear viscosity decreases as the channel width increases and has its bulk value at the $h = 6.3$ nm channel. Calculated shear viscosity values for
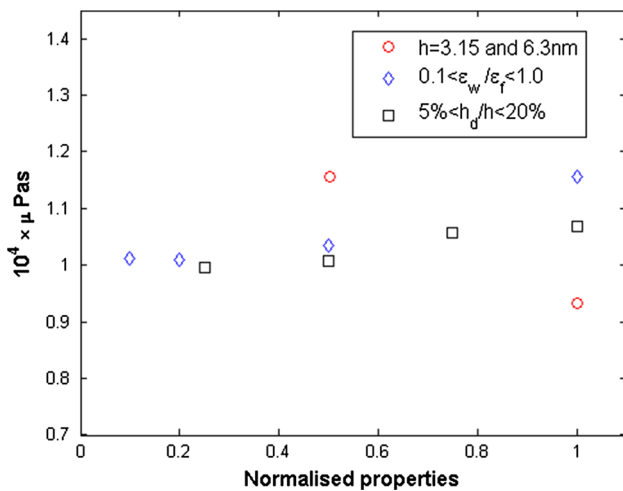
Fig. 2 Shear viscosity values investigated versus the effect of various parameters, such as channel height, wall wettability ratio, and roughness height. Each parameter on the *horizontal axis* is normalized to its maximum value for presentation reasons

argon presented here are in good agreement with values reported in the literature for flat-wall channels (Ashurst and Hoover 1975; Ohara and Suzuki 2001; Pas and Zwolinski 1991).

The diagram reveals a monotonic increase in shear viscosity past a wall with increased hydrophilicity. On the other hand, hydrophobic walls give rise to lower shear viscosity values, which is in agreement with slip length calculations in the literature, where a viscosity layer adjacent to the wall exists and correlates with slippage over a hydrophobic surface (Vinogradova 1995; Cao et al. 2009; Myers 2011).

We also report increasing shear viscosity values as wall groove height increases from 5 to 20 %h (for the $h = 6.3$ nm channel) as expected, since, practically, an increase in h_d resembles a channel width decrease.

3.2 Friction factor

In Fig. 3a, we present a fully logarithmic plot of f versus Re for two flat-wall channels, of width $h = 3.15$ nm and $h = 6.3$ nm. The two channels are investigated for the same values of the dimensionless group $\Pi_\varepsilon = \varepsilon_w/\varepsilon_f$. We observe that the data points are well organized in power-law curves for each wettability ratio. No channel size effect is observed, as one would expect based on our dimensional analysis arguments. A power-law least-squares approximation of the form $f = bRe^a$ represents the data very well. The value of parameter a is very close to -1, and consequently, a correlation of the form $f = \frac{b}{Re}$ approximates data fairly good. Such an approximation would lead to the conclusion that the constancy of Poiseuille number, that holds
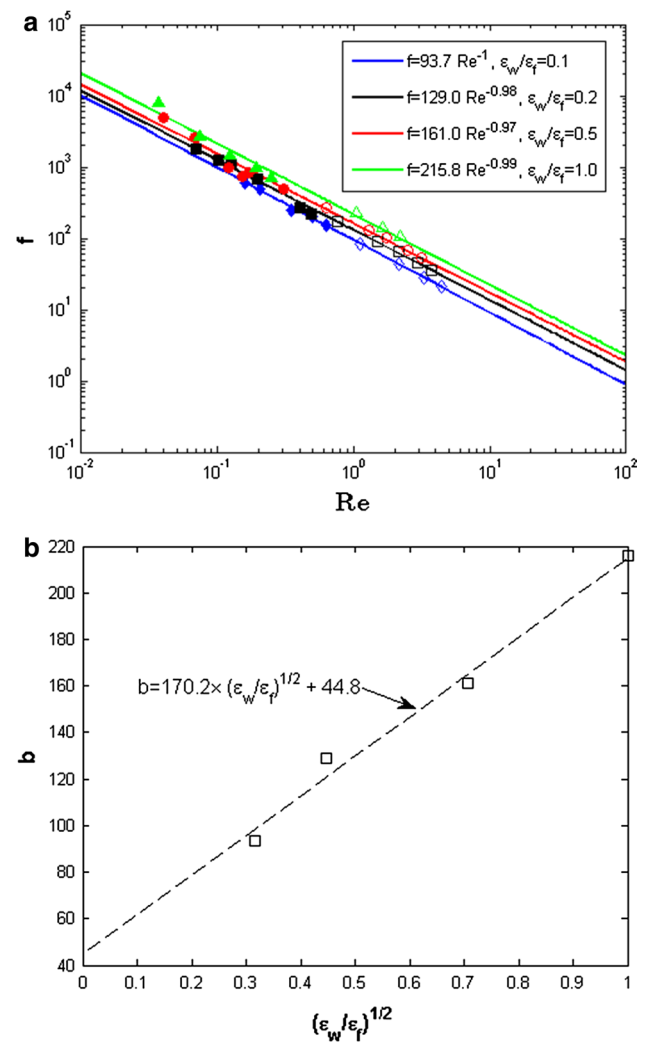

Fig. 3 a Friction factor f for two flat-wall channels of width $h = 3.15$ and 6.3 nm for various $\varepsilon_w/\varepsilon_f$ ratios. *Filled symbols* represent $h = 3.15$ nm and *empty symbols* $h = 6.3$ nm data points. *Lines* are power-law least-squares fits, **b** correlation of parameter b with wettability parameter $\sqrt{\varepsilon_w/\varepsilon_f} = \varepsilon_{wf}/\varepsilon_f$

for laminar flow in macrochannels, is also valid in the case of nanochannel flows, provided that b is now understood as depending on $\varepsilon_w/\varepsilon_f$. However, we restrain from adopting this approximation (here and in the remainder of the paper) in order to report only the best approximations (in the least-squares sense) to our computed values of friction factor.

Figure 3b presents the dependence of parameter b on $\sqrt{\varepsilon_w/\varepsilon_f}$. A linear fit seems to apply well on the data points ($R^2 = 0.987$) yielding the relationship $b = 170.2\varepsilon_{wf}/\varepsilon_f + 44.8 = 170.2\sqrt{\varepsilon_w/\varepsilon_f} + 44.8$, for flat-wall channels.

To elaborate on the different effects of roughness elements and blocking elements, we examine the flow characteristics for various h_d/h, fixed $\varepsilon_w/\varepsilon_f = 0.1$ (hydrophobic channel walls) for $h = 3.15$ nm and $h = 6.3$ nm. Figure 4
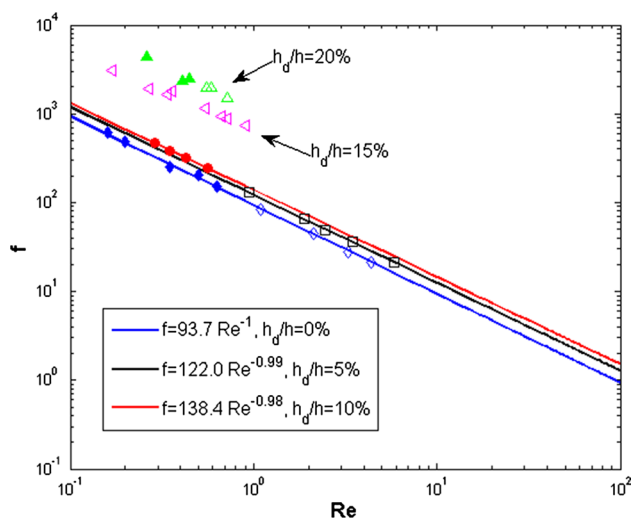
Fig. 4 Friction factor f versus Re for various h_d/h ratios and $\varepsilon_w/\varepsilon_f = 0.1$. *Filled symbols* represent $h = 3.15$ nm and *empty symbols* $h = 6.3$ nm data points. *Lines* are power-law least-squares fits

depicts the calculated f values for protrusion heights $h_d = 0\,\%h$ (flat-wall), $h_d = 5$ and $10\,\%h$ as well as $h_d = 15$ and $20\,\%h$. Note that no data points for $h = 3.15$ nm exist for $h_d = 5$ and $15\,\%h$ as the channel upper wall morphology is impossible for the specific channel-height/groove-height ratio. Evidently, protrusions of height greater than $15\,\%h$ generate highly perturbed flow fields which, in turn, lead to values of f that are materially affected by the size (scale) of the channel. Similar diagrams are obtained for other $\varepsilon_w/\varepsilon_f$ ratios. To differentiate between the two cases, we use here the term grooved nanochannels (for $h_d \geq 15\,\%h$) in contradistinction with the rough-wall nanochannels (for $h_d \leq 10\,\%h$) considered before.

Moreover, we observed that the power-law coefficient a in $f = bRe^a$ deviates from -1 ($a = -1 \pm 0.1$, within statistical error) in hydrophilic channels with $h_d > 10\,\%h$. This is evidence that a hydrophilic wall in a channel with groove height comparable to channel height can induce irregularities that make the constancy of the Poiseuille number not valid.

The trend that the friction factor decreases as the channel walls become more hydrophobic persists in the case of rough- and grooved-wall nanochannels. However, as shown in Cao et al. (2006) the combined effect of wall roughness and hydrophobicity on friction factor is not a monotonic function.

4 Conclusions

We believe that the fact that the friction factor values (computed based on the output of MD simulations) are organized on well-defined curves lends strong support to the choice of the most relevant dimensional parameters for the family of nanoflows studied. These friction factor curves are approximated very well by power laws of the form $f = bRe^a$ when either h_d/h or $\varepsilon_w/\varepsilon_f$ is kept constant.

Based on the MD simulations, we constructed diagrams and developed correlations that are useful in estimating the friction factor over a range of Reynolds number values relevant to nanoflows. These diagrams allow one to estimate the effect that the wettability ratio (as expressed by the ratio $\varepsilon_w/\varepsilon_f$) has on f. As a rule (at least in all cases investigated in this work), the friction factor decreases as the channel walls become more hydrophobic. The influence of the relative protrusion height on the friction factor was also quantified. Nanoconduits with wall protrusions of relative height (h_d/h) up to 10 % can be classified as rough-wall nanochannels. Above this threshold value, nanoconduits with protrusions of relative height 15, 20 % and higher should be classified as grooved.

Summarizing, the MD results show a dependence of friction factor not only on geometric characteristics, e.g., h_d/h, but also on the nature of interactions between the fluid and the walls (through the $\varepsilon_w/\varepsilon_f$ parameter), and the behavior of friction factor is approximated very well by power law of the form $f = bRe^a$. As a result, one can expect that the knowledge of such relations can lead to tailor-made nanochannels leading to lower power loses, an issue that is important for nanodevices where energy consumption is an important issue. The friction factor predicted by the proposed correlation can be used in conceptual preliminary and even advanced stages of design. The detailed relations that can be extracted from MD simulations could be incorporated in a multiscale design tool for nanodevices incorporating nanochannels, since they would take into account both geometry and surface fluid interactions.

References

Ashurst WT, Hoover WG (1975) Dense-fluid shear viscosity via non-equilibrium molecular dynamics. Phys Rev A 11:658–678

Asproulis N, Drikakis D (2011) Wall mass effects on hydrodynamic boundary slip. Phys Rev E 84:031504

Asproulis N, Drikakis D (2013) An artificial neural network-based multiscale method for hybrid atomistic-continuum simulations. Microfluid Nanofluid 15:559–574

Asproulis N, Kalweit M, Drikakis D (2012) A hybrid molecular continuum method using point wise coupling. Adv Eng Softw 46:85–92

Bernardo P, Drioli E, Golemme G (2009) Membrane gas separation: a review/state of the art. Ind Eng Chem Res 48:4638–4663

Cao BY, Chen M, Guo ZY (2006) Liquid flow in surface-nanostructured channels studied by molecular dynamics simulation. Phys Rev E 74:066311

Cao BY, Sun J, Chen M, Guo ZY (2009) Molecular momentum transport at fluid–solid interfaces in MEMS/NEMS: a review. Int J Mol Sci 10:4638–4706

Cao BY, Li Y-W, Dong R-Y, Kong J, Chen H, Xu Y, Yung K-L (2011) Superhydrophobicity of self-organized surfaces of polymer nanowire arrays fabricated by a nano-injection moulding technique. J Therm Sci Technol Jpn 6:204–209

Cottin-Bizonne C, Barentin C, Bocquet L (2012) Scaling laws for slippage on superhydrophobic fractal surfaces. Phys Fluids 24:012001

Davies J, Maynes D, Webb BW, Woolford B (2006) Laminar flow in a microchannel. Phys Fluids 18:087110

Delhommelle J, Petravic J, Evans DJ (2004) Non-Newtonian behavior in simple fluids. J Chem Phys 120:6117–6123

Gargiuli J, Shapiro E, Gulhane H, Nair G, Drikakis D, Vagdama P (2006) Microfluidic systems for in situ formation of nylon 6,6 membranes. J Membr Sci 282:257–265

Giannakopoulos AE, Sofos F, Karakasidis TE, Liakopoulos A (2012) Unified description of size effects of transport properties of liquids flowing in nanochannels. Int J Heat Mass Transf 55:5087–5092

Grannick S (1991) Motions and relaxations of confined liquids. Science 253:1374–1379

Herwig H, Gloss D, Wenterodt T (2008) A new approach to understanding and modeling the influence of wall roughness on friction factors for pipe and channel flows. J Fluid Mech 613:35–53

Kalweit M, Drikakis D (2010) On the behavior of fluidic material at molecular dynamics boundary conditions used in hybrid molecular-continuum simulations. Mol Simul 36:657–662

Kandlikar SG, Schmitt D, Carrano AL, Taylor JB (2005) Characterization of surface roughness effects on pressure drop in single phase flow in minichannels. Phys Fluids 17:100606

Kleinstreuer C, Li J, Koo J (2008) Microfluidics of nano-drug delivery. Int J Heat Mass Transf 51:5590–5597

Koplik J, Banavar JR (2006) Slip, immiscibility, and boundary conditions at the liquid-liquid interface. Phys Rev Lett 96:044505

Koplik J, Banavar JR, Willemsen J (1988) Molecular dynamics of Poiseuille flow and moving contact lines. Phys Rev Lett 60:1282–1285

Markesteijn AP, Hartkamp R, Luding S, Westerweel J (2012) A comparison of the value of viscosity for several water models using Poiseuille flow in a nano-channel. J Chem Phys 136:134104

Maynes D, Jeffs K, Woolford B, Webb BW (2007) Laminar flow in a microchannel with hydrophobic surface patterned microribs oriented parallel to the flow direction. Phys Fluids 19:093603

Moody LF (1944) Friction factors for pipe flow. ASME Trans J Appl Mech 66:671–677

Myers TG (2011) Why are slip lengths so large in carbon nanotubes? Microfluid Nanofluid 10:1141–1145

Nikuradse J (1933) Laws of flow in rough pipes ["Stromungsgesetze in Rauen Rohren," VDI-Forschungsheft 361]

Noy A, Park HG, Fornasiero F, Holt JK, Grigoropoulos CP, Bakajin O (2007) Nanofluidics in carbon nanotubes. Nano Today 2:22–29

Ohara T, Suzuki D (2001) Intermolecular momentum transfer in a simple liquid and its contribution to shear viscosity. Microsc Thermophys Eng 5:117–130

Pas MF, Zwolinski BJ (1991) Computation of the transport coefficients of dense fluid neon, argon, krypton and xenon by molecular dynamics. Mol Phys 73:471–481

Priezjev NV (2007) Effect of surface roughness on rate-dependent slip in simple fluids. J Chem Phys 127:144708

Ritos K, Mattia D, Calabro F, Reese JM (2014) Flow enhancement in nanotubes of different materials and lengths. J Chem Phys 140:014702

Sbragaglia M, Benzi R, Biferale L, Succi S, Toschi F (2006) Surface roughness–hydrophobicity coupling in micro and nanochannel flows. Phys Rev Lett 97:204503

Sofos F, Karakasidis TE, Liakopoulos A (2009) Transport properties of liquid argon in krypton nanochannels: anisotropy and non-homogeneity introduced by the solid walls. Int J Heat Mass Trans 52:735–743

Sofos F, Karakasidis TE, Liakopoulos A (2010) Effect of wall roughness on shear viscosity and diffusion in nanochannels. Int J Heat Mass Trans 53:3839–3846

Sofos F, Karakasidis TE, Liakopoulos A (2012) Surface wettability effects on flow in rough wall nanochannels. Microfluid Nanofluid 12:25–31

Thomas JA, McGaughey AJH (2007) Effect of surface wettability on liquid density, structure, and diffusion near a solid surface. J Chem Phys 126:034707

Tretheway DC, Meinhart CD (2002) Apparent fluid slip at hydrophobic microchannel walls. Phys Fluids 14:L9–L12

Valdés JR, Miana MJ, Martínez M, Gracia L, Pütz T (2007) Numerical investigation of the influence of roughness on the laminar incompressible fluid flow through annular microchannels. Int J Heat Mass Transf 50:1865–1878

Valdés JR, Miana MJ, Martínez M, Gracia L, Pütz T (2008) Introduction of a length correction factor for the calculation of laminar flow through microchannels with high surface roughness. Int J Heat Mass Transf 51:4573–4582

Vinogradova OI (1995) Drainage of a thin liquid-film confined between hydrophobic surfaces. Langmuir 11:2213–2220

Voronov RS, Papavassiliou DV, Lee LL (2006) Boundary slip and wetting properties of interfaces: correlation of the contact angle with the slip length. J Chem Phys 124:204701

Walther JH, Ritos K, Cruz-Chu ER, Megaridis CM, Koumoutsakos P (2013) Barriers to superfast water transport in carbon nanotube membranes. Nano Lett 13:1910–1914

Ybert C, Barentin C, Cottin-Bizonne C, Joseph P, Bocquet L (2007) Achieving large slip with superhydrophobic surfaces. Phys Fluids 19:123601

Zhu Y, Granick S (2002) Limits of the hydrodynamic no-slip boundary condition. Phys Rev Lett 88:106102